Biomacromolecules

pubs.acs.org/Biomac Article

Modeling and Designing Particle-Regulated Amyloid-like Assembly of Synthetic Polypeptides in Aqueous Solution

Tianjian Yang, Kyle Benson, Hailin Fu, Tianrui Xue, Ziyuan Song, Hanyi Duan, Hongwei Xia, Ankarao Kalluri, Jie He, Jianjun Cheng,* Challa V. Kumar,* and Yao Lin*

Cite This: https://doi.org/10.1021/acs.biomac.1c01230 Read Online

ACCESS | Metrics & More | Article Recommendations | Supporting Information

ABSTRACT: In cells, actin and tubulin polymerization is regulated by nucleation factors, which promote the nucleation and subsequent growth of protein filaments in a controlled manner. Mimicking this natural mechanism to control the supramolecular polymerization of macromolecular monomers by artificially created nucleation factors remains a largely unmet challenge. Biological nucleation factors act as molecular scaffolds to boost the local concentrations of protein monomers and facilitate the required conformational changes to accelerate the nucleation and subsequent polymerization. An accelerated assembly of synthetic poly(L-glutamic acid) into amyloid fibrils catalyzed by cationic silica nanoparticle clusters (NPCs) as artificial nucleation factors is demonstrated here and modeled as supramolecular polymerization with a surface-induced heterogeneous nucleation pathway. Kinetic studies of fibril growth coupled with mechanistic analysis demonstrate that the artificial nucleators predictably accelerate the supramolecular polymerization process by orders of magnitude (e.g., shortening the assembly time by more than 10 times) when compared to the uncatalyzed reaction, under otherwise identical conditions. Amyloid-like fibrillation was supported by a variety of standard characterization methods. Nucleation followed a Michaelis−Menten-like scheme for the cationic silica NPCs, while the corresponding anionic or neutral nanoparticles had no effect on fibrillation. This approach shows the effectiveness of charge−charge interactions and surface functionalities in facilitating the conformational change of macromolecular monomers and controlling the rates of nucleation for fibril growth. Molecular design approaches like these inspire the development of novel materials via biomimetic supramolecular polymerizations.

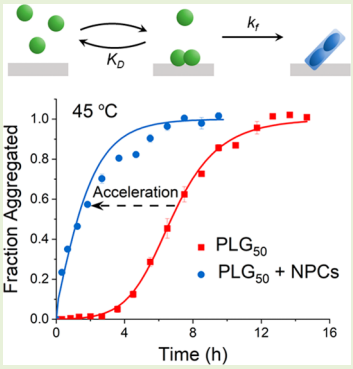

INTRODUCTION

Much progress has been made in nucleating, activating, and accelerating the cooperative assembly of synthetic organic molecules into supramolecular polymers.[1−12] This progress takes advantage of the in-depth understanding of rate-limiting, supramolecular "nucleation" processes and noncovalent bonding interactions among supramolecular reagents.[13−17] Even so, regulating the assembly of synthetic macromolecular subunits into supramolecular polymer structures remains challenging. This is due to the complexity in synthesizing artificial nucleators that have sizes comparable to those of macromolecular monomers and that can interact with these subunits in an effective way to catalyze polymerizations. This task is even more difficult in aqueous media, as supramolecular monomers and nucleators compete with water in forming hydrogen-bonded complexes. In addition, the large dielectric constant of water renders the electrostatic field effect a relatively short-ranged interaction. A majority of current approaches for the assembly of synthetic macromolecular monomers carried out in aqueous solutions are either slow[18−22] (e.g., due to the kinetic barriers or required conformational changes) or rely on the amphiphilic design of the macromolecular monomers.[23−29] The latter usually needs the assistance of an organic solvent in the assembly process[30−35] or requires environmental stimuli or reactions that modulate monomer solubility to facilitate the assembly.

In contrast, supramolecular assembly of proteins into large filamentous polymers in water is ubiquitous in cells and strictly regulated by a variety of protein complexes called nucleation factors.[36−38] For example, formins and the actin-related protein-2/3 (Arp2/3) complex can accelerate actin polymerization by locally promoting the formation of oligomeric nuclei required for actin filament growth.[36,39] In the absence of these nucleation factors, both nucleation and polymerization proceed very slowly. These protein nucleators can be regarded as a class of macromolecular machines which take advantage of their sophisticated, multidomain structures to concentrate protein subunits and catalyze nucleation. Interestingly, a variety of foreign particles and interfaces have also been reported to

Received: September 17, 2021
Revised: December 7, 2021

promote the nucleation and growth of β-amyloid fibrils via the supramolecular assembly of misfolded proteins or their fragments.[40−43] The nucleator-like effect of these particles, albeit limited, may be facilitated by high local concentrations of proteins adsorbed on the particle surface, rapid clustering in confined spaces, and/or favorable changes in the protein structure induced by interactions with the particle surface.[40,43−45] In the early evolution of protein-based nucleator factors, their ability to concentrate protein subunits and catalyze nucleation was also likely to be primitive and improved via natural selection. By mimicking the fundamental principles of biological supramolecular polymerization, synthetic nucleation factors may be developed from nanoparticular or macromolecular platforms by an iterative process of design, analysis, and refinement.

During the discovery of protein nucleators, kinetic modeling has played a major part in elucidating their mechanism in regulating protein polymerization.[13,14,36,46−48] More recently, the extensive kinetic studies on the reaction processes underlying the formation of disease-related amyloid fibrils from proteins and soluble peptides have yielded a unified modeling framework accounting for the intrinsic catalytic nature of protein aggregation.[17,48−50] Almost every fundamental process (e.g., nucleation, propagation, and secondary processes) is likely to exhibit an enzyme-like saturation effect and may be approximately described by a Michaelis−Menten-like rate law.[51] This is an important conceptual breakthrough, as in the present study, and many complex processes involved in the protein and peptide assembly may now be analyzed by an intuitive modeling framework with fewer parameters.

Inspired by this recent development, we envisioned that the nucleator-like effect of particles may also be found in the assembly of certain synthetic polypeptides without a specific sequence, and more importantly the process may be described by a similar minimalist kinetic framework. Synthetic polypeptides prepared from precision synthesis, for example, by controlled ring-opening polymerization of amino acid *N*-carboxyanhydride (NCA), have been widely used as protein mimics, and their applications in biomaterial and biomedical areas have steadily increased over the years.[52−54] Numerous polypeptide-containing macromolecules with controlled compositions and architectures have been synthesized for predictable conformational structures and tunable interactions in solution and in assemblies.[18,55−58] As these polypeptides have major potential in biology-related applications, it is noteworthy to learn how a simple nanoparticle (NP) surface may provide some primitive regulation for polypeptide assembly in aqueous solution. It is worth identifying the minimal requirements for designing a primitive artificial nucleator for these macromolecular subunits in aqueous solution and develop a kinetic model that accounts for every fundamental process of regulated assembly with minimal number of parameters. This effort is necessary to approach new pathways toward the spatial and temporal regulation of assembly of synthetic polypeptides or other "foldable" macromolecules.

Herein, we first introduce a kinetic model that considers particle-induced heterogeneous nucleation as a two-step Langmuir/Michaelis−Menten-like process and demonstrate how a nucleator-like behavior may provide the kinetic control over the assembly of polypeptides in aqueous solution. We then validate this model by analyzing the aggregation behavior of poly(L-glutamic acid)s (PLGs) accelerated by cationic silica nanoparticle clusters (NPCs), comprising multiple NPs. Using synthetic homopolypeptides eliminates the sequence-specific complexities of previous studies on proteins or β-sheet-forming peptides. The cationic NPCs accelerate the assembly of ionic PLGs by providing a localized heterogeneous nucleation pathway, a process which is predictable using the proposed kinetic model. The strategy is particularly suitable for the kinetic pathway in which the refolding process required for oligomerization is the rate-limiting step of nucleation. Multiple control experiments were performed to support our proposed mechanism. Additionally, we will discuss some additional considerations on how to design more sophisticated synthetic nucleators.

MATERIALS AND METHODS

Materials. Amino acids were purchased from Chem-Impex International Inc. (Wood Dale, IL, USA). Deuterated solvents were purchased from Cambridge Isotope Laboratories, Inc. (Tewksbury, MA, USA). Anhydrous dichloromethane (DCM) was stored over 3 Å molecular sieves in a freezer. Sodium acetate buffer, (3-aminopropyl)-triethoxysilane (APTES), hydrochloric acid (HCl), sodium hydroxide (NaOH), trifluoroacetic acid (TFA), and dimethylformamide (DMF) were purchased from Sigma-Aldrich (Milwaukee, WI, USA). Thioflavin T (ThT) and potassium bromide were obtained from Acros Organics (New Jersey, USA). Silicon dioxide nanopowder was purchased from US Research Nanomaterials, Inc. (Houston, TX, USA). 0.2 μm nylon or PTFE syringe filters were purchased from GE Healthcare (Chicago, IL, USA). 96-well half-area, clear bottom, and nonbinding microplates and microplate sealing tapes were purchased from Corning Inc. (Corning, NY, USA).

Instrumentation. Nuclear magnetic resonance spectra were recorded on a DMX 500 MHz spectrometer (Bruker Corporation, Billerica, MA, USA) for polymer characterization. Tandem gel permeation chromatography (GPC) experiments of poly(ϵ-benzyloxycarbonyl-L-lysine) (PZLL) polymers were performed on a system equipped with an isocratic pump (model 1100, Agilent Technology, Santa Clara, CA, USA), a DAWN HELEOS 18-angle laser light scattering detector [also known as multi-angle laser light scattering (MALLS) detector, Wyatt Technology, Santa Barbara, CA, USA], and an Optilab rEX refractive index detector (Wyatt Technology, Santa Barbara, CA, USA). The detection wavelength of HELEOS was set at 658 nm. Separations were performed using serially connected size exclusion columns (100, 500, 103, and 10^4 Å Phenogel columns, 5 μm, 300 × 7.8 mm, Phenomenex, Torrance, CA, USA) at 60 °C using DMF containing 0.1 M LiBr as the mobile phase. The MALLS detector was calibrated using pure toluene, with no need for external polymer standards, and can be used for the determination of the absolute molecular weights (MWs) of polymers. GPC data of poly(γ-benzyl-L-glutamate) (PBLG) polymers were collected via an instrument equipped with an isocratic pump (1260 Infinity II, Agilent, Santa Clara, CA, USA), a multi-angle static light scattering (MALS) detector with the detection wavelength at 658 nm (DAWN HELEOS-II, Wyatt Technology, Santa Barbara, CA, USA), and a differential refractometer detector (Optilab T-rEX, Wyatt Technology, Santa Barbara, CA, USA). Separations were performed by serially connected size exclusion columns (three PLgel MIXED-B columns, 10 μm, 7.5 × 300 mm, Agilent, Santa Clara, CA, USA), which were maintained at 40 °C using DMF containing 0.1 M LiBr as the mobile phase at a flow rate of 0.7 mL/min. The MALS detector was calibrated using pure toluene and then was used for the determination of the absolute MWs. All sample solutions were filtered by a 0.45 μm PTFE filter before injection. The MWs of polypeptides were determined based on the dn/dc value of each sample calculated offline by using the internal calibration system processed by the software ASTRA 7 (version 7.1.3.15, Wyatt Technology, Santa Barbara, CA, USA). Fourier transform infrared (FTIR) spectra were obtained using a PerkinElmer 100 serial FTIR spectrophotometer (PerkinElmer, Santa Clara, CA, USA) which was calibrated with a polystyrene film.

https://doi.org/10.1021/acs.biomac.1c01230
Biomacromolecules XXXX, XXX, XXX−XXX

Dynamic light scattering (DLS) studies of SiO_2−NH_2 NPCs were carried out on an ALV compact goniometer system with a 90° detector (CGS-3MD) (Germany), which consists of a 22 mW He−Ne laser (emitting vertically polarized light with a wavelength of 632.8 nm). SiO_2−NH_2 NPCs were dispersed in 15 mM sodium acetate buffer with pH 4.0 for characterizations. The zeta potential of SiO_2−NH_2 NPCs was measured using the laser Doppler velocimetry method in a ZetaPlus zeta potential analyzer (Brookhaven Instruments Corporation, Holtsville, NY, USA). Zeta potentials were measured in a 4 mL polystyrene cuvette, with at least three replicates for each sample, and analyzed by using the Smoluchowski equation. Circular dichroism (CD) spectra were measured by a Chirascan V100 spectropolarimeter (Applied Photophysics, Leatherhead, Surrey, UK) and a quartz cuvette with either 1 or 3 mm path length. Temperature was controlled by a Peltier holder. Attenuated total reflection infrared spectroscopy (FTIR−ATR) was carried out using a Nicolet Magna 560 spectrometer equipped with a diamond ATR element (Thermo Fisher Sci., Waltham, MA, USA). The ATR spectra of the freeze-dried samples were obtained with 4 cm^{-1} resolution and 64 co-averages. UV−vis spectra were measured using a Nanodrop 2000 spectrometer (Thermo Fisher Sci., Waltham, MA, USA) with a path length of 1 mm. Morphologies of the amyloid assemblies were characterized by a Tecnai T12 G2 Spirit BioTWIN (Thermo Fisher Sci., Waltham, MA, USA) transmission electron microscope (TEM) operating at an accelerating voltage of 80 kV. Sample solutions were deposited on TEM grids, blotted by a filter paper, and allowed to dry under ambient conditions. The carbon-coated copper grids (carbon film 200 mesh copper, Ted Pella Inc., Redding, CA, USA) were pretreated with plasma for 15 s (Harrick Plasma PDC-32G, Harrick Plasma, Ithaca, NY, USA) before loading samples. The morphologies of the amyloid structure and NPCs were also characterized with a FEI Nova NanoSEM 450 (Thermo Fisher Sci., Waltham, MA, USA) field emission scanning electron microscope with an accelerating voltage of 1 kV. Amyloid assembly samples were deposited on TEM grids and then coated with another layer of platinum before imaging. The cationic NPC sample was deposited on TEM grids without coating before imaging. Wide-field fluorescence microscopy experiments were performed on an Andor confocal microscope (Oxford Instrument Andor, Belfast, Northern Ireland). The excitation wavelength was chosen at 488 nm and the detection wavelength at 509 nm. Before the experiments, the supramolecular assemblies were stained with ThT. ThT-based fluorescence assays were performed using a FlexStation 3 microplate reader (Molecular Devices, San Jose, CA, USA). The pH values of all the solutions were measured by an Orion 8103BNUWP ROSS Ultra pH electrode (Thermo Fisher Sci., Waltham, MA, USA) and adjusted to the targeted values.

Synthesis of PLG Polymers. PBLG was synthesized by NCA polymerization using hexylamine as the initiator using previously reported methods.[59,60] GPC characterization indicated a well-defined polypeptide structure ($PBLG_{50}$, M_n = 11.0 kDa, $Đ$ = 1.05; $PBLG_{85}$, M_n = 19.2 kDa, $Đ$ = 1.05). To deprotect PBLG to obtain PLG, PBLG (80 mg, 0.36 mmol benzyl groups) was dissolved in DCM at room temperature, into which fresh iodotrimethylsilane (312 μL, 2.19 mmol) was added through a syringe under nitrogen protection. The solution was stirred at room temperature for 24 h. After precipitation by the addition of ether (40 mL), $NaHCO_3$ saturated solution (4 mL) was added to dissolve the solid residue. The byproduct benzyl iodide was removed by extraction with ether (3 × 3 mL). The product PLG was purified by dialysis (MWCO = 1 kDa) for 48 h, followed by lyophilization.

Synthesis of Poly(L-lysine) Polymers. Poly(ε-carboxybenzyl-L-lysine) (PZLL) was synthesized by NCA polymerization using hexylamine as the initiator using previously reported methods.[59,60] GPC characterization indicated a well-defined polypeptide structure ($PZLL_{298}$, M_n = 78.0 kDa, $Đ$ = 1.20). For the deprotection of PZLL, PZLL (70 mg, 0.27 mmol benzyl groups) was dissolved in TFA at 0 °C in an ice bath, into which the HOAc solution of HBr (33 wt %, 234 μL, 1.33 mmol) was added through a syringe. The solution was stirred at 0 °C for 2 h. After the removal of solvent by precipitation in ether (40 mL), HCl solution (0.1 M, 2 mL) and DI water (2 mL) were added to dissolve the solid residue. The byproduct benzyl bromide was removed by extraction with ether (3 × 3 mL). The product poly(L-lysine) (PLL) was purified by dialysis (MWCO = 1 kDa) for 48 h, followed by lyophilization.

Synthesis of Cationic Silica NPCs. Cationic NPCs were synthesized by the surface modification of bare silica NPs with APTES by modified established methods.[61,62] Silica NP powder (d ∼ 20 nm, 100 mg) was dispersed in a mixture of DI water (90 mL) and methanol (100 mL) in a round-bottom flask by sonicating for 0.5 h with an ice bag, into which the mixture of ammonium hydroxide (28%, 15 mL) and methanol (20 mL) was added. The resulting dispersion was functionalized by adding APTES (15 mL in 30 mL of methanol) dropwise with stirring. The mixture was allowed to stir and reflux at 70 °C for 4 h. The product NPs were purified by centrifugation and redispersion for two times in isopropanol, followed by two times in 5 mM HCl. The product cationic silica NPCs was vacuum-dried for 12 h at room temperature. From DLS, it is observed that the dispersion of cationic silica NPCs has an average hydrodynamic diameter of 130 nm (Figure S5c,d), which is a suitable size for equilibrium binding studies with PLG by the centrifugation assay. The clustered structure of cationic silica NPCs increases the surface area-to-volume ratio for maximized binding capacity.

Binding Isotherms of PLGs on NPCs. The dissociation equilibrium constant (K_D) and the binding capacity of PLG_{50} to NPCs at 25, 45, and 75 °C were measured by UV−vis-based centrifugation assay. Briefly, stock solutions of PLG_{50} sodium salt (0.53 mM) and NPC (2 mg/mL) were prepared in filtered 15 mM sodium acetate buffer. If necessary, the stock solutions were adjusted with filtered 1 M HCl to achieve a final pH of 4.0. NPCs were sonicated until they were evenly dispersed in solution. Working solutions consisting of 0−73.8 μM of PLG_{50} and 0.4 mg/mL of NPCs were prepared in Eppendorf PCR tubes on ice by combining appropriate volumes of the stock solutions and diluting with 15 mM sodium acetate, pH 4.0. After incubation in a water bath at a set temperature for 10 min, the NPCs and bound PLG_{50} were removed by centrifugation. Free PLG concentrations were quantified by UV absorbance at 209 nm. Bound PLG concentrations were determined by subtracting the free PLG concentrations from the total concentrations. Each analyte solution was prepared at least in triplicate. K_D and the binding capacity were determined by fitting the experimental data with the Langmuir binding isotherm model with a single type of independent sites. Studies on the binding of PLL_{298} to PAA−AuNPs was carried out in a similar way.

Assembly Kinetics of PLGs Monitored by Ex Situ ThT Fluorescence Assays. The solutions were prepared by combining appropriate volumes of the PLG_{50} and NPC stock solutions and diluting with 15 mM sodium acetate, pH 4.0, in low-binding Eppendorf tubes on ice. Each condition was prepared at least in triplicate. 60 μM ThT stock solution in 15 mM sodium acetate, pH 4.0, was filtered prior to use. To initiate the amyloid assembly, PLG solutions were incubated in water bath at 45 or 75 °C. 15 μL of the reaction aliquot was removed at intervals and immediately combined with 75 μL of 60 μM ThT in a Corning 3881 96-well half-area, clear bottom, and nonbinding microplate. ThT emission spectra were obtained using a FlexStation 3 plate reader at 25 °C with excitation at 440 nm. The linear relationship between the ThT fluorescence intensity and the mass concentration of PLG_{50} amyloid fibrils was validated by carrying out a series of control experiments (see the Materials and Methods section). Fluorescence intensities at 485 nm were used to obtain the time progress kinetic profile.

Kinetic Data Processing. The calibration experiments show an excellent linear correlation between the ThT fluorescence and the mass concentration of PLG_{50} amyloid fibrils. To calculate the fraction aggregated at a given time, fluorescence intensities at 485 nm for each sampling point in a kinetic trace were normalized by the final fluorescence intensity at equilibrium. All the kinetic profiles in Figures 4, 7, and S8 are from the average of three independent experiments, showing a good reproducibility of the measurements.

Kinetic Modeling. The differential rate equations were solved numerically using ode15s or ode45 in MATLAB. The rate constants

https://doi.org/10.1021/acs.biomac.1c01230
Biomacromolecules XXXX, XXX, XXX−XXX

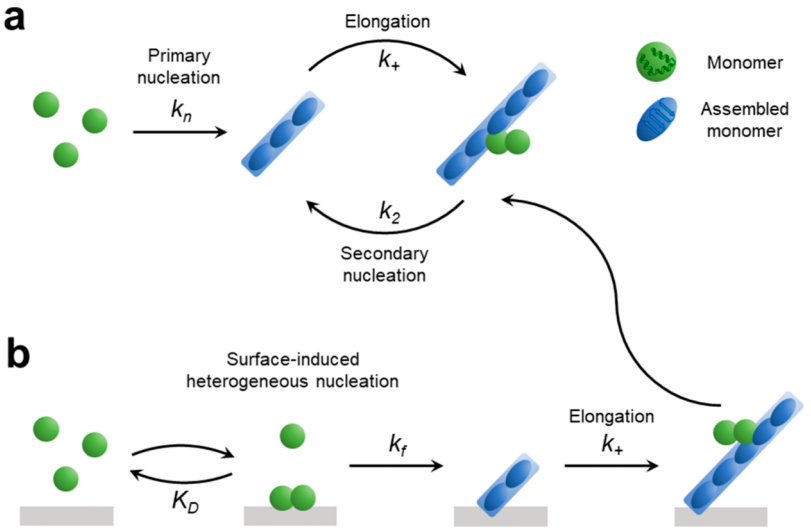

Figure 1. Schematic illustration of the kinetic model for supramolecular assembly of synthetic polypeptides regulated by the NP surface. (a) In the absence of particle-based nucleators, the amyloid-like fibrillation of polypeptides in solution follows a classic nucleation−elongation pathway. In addition to the spontaneous primary nucleation, a secondary nucleation process may occur on the surface of the existing fibrils to initiate the growth of new fibrils. (b) In the presence of particle-based nucleators, the primary nucleation may occur through a heterogeneous nucleation pathway facilitated by the particle surface, where the nuclei formation is promoted by the interaction between the polypeptide monomers and the particle surface.

were obtained by minimizing the sum of squared error between the simulated results and the experimental data. See the Supporting Information for sample scripts written in MATLAB.

Monitoring the Refolding of PLGs and PLLs in the Assembly Process by CD Spectroscopy. Time-dependent CD spectra of PLG solutions in the absence or presence of various types of NPs were collected at intervals of 10 min, scanning from 200 to 250 nm with 1 nm of wavelength step. Solutions were prepared in a similar way as mentioned in ThT fluorescence assays. The solution was sealed in a quartz cuvette with 1 mm path length and incubated in a Peltier holder set to a specific temperature. Background signals were subtracted using an appropriate buffer solution. Studies on PLLs were carried out in a similar way.

Supramolecular Assembly Kinetics of PLGs Monitored by in Situ ThT Fluorescence Assays. PLG sodium salt (4 mg/mL, 0.53 mM), NPCs (2 mg/mL), and ThT (500 μM) stock solutions were prepared in filtered (0.22 μm Nylon syringe filter) 15 mM sodium acetate. The pH of stock solutions was tuned to 4.0 using 1 M HCl. The reaction solutions were prepared by combining appropriate volumes of the stock solutions and diluting with 15 mM sodium acetate, pH 4.0, in low-binding Eppendorf tubes on ice. Each reaction solution also contained 50 μM of ThT as the in situ fluorescent probe. The samples were pipetted into multiple wells of a Corning 3881 microplate, 100 μL per well. Each kinetic group was prepared and measured at least in triplicate. The microplates were sealed by Corning 6575 optical adhesive tapes, and the supramolecular polymerization was initiated by placing the microplate at 45 °C in a FlexStation 3 plate reader. The ThT fluorescence was recorded every 7 min using the bottom reading mode with 440 nm excitation, 485 nm emission, and 455 nm cutoff filters. The plate reader shook the microplates for 20 s prior to each measurement.

RESULTS AND DISCUSSION

Kinetic Model of Particle-Regulated Amyloid Assembly

We consider a kinetic model for amyloid fibrillation of polypeptides in the presence and absence of particle-based artificial nucleators (Figure 1). In the absence of nucleators, the assembly of proteins and peptides into amyloid fibrils was usually modeled as a two-stage, nucleated polymerization process (Figure 1a) by considering a homogeneous nucleation pathway, in which fibril growth follows the spontaneous formation of primary nucleus, as well as a secondary pathway, for example, a secondary nucleation process in which the surface of existing fibrils initiates growth of new fibrils or a fragmentation process of the fibrils which increase the number of growing chains.[48,63] We focus on the secondary nucleation process here as it is more relevant for the assembly of synthetic polypeptides without vigorous stirring,[64] and the mathematics can be readily extended to fragmentation or other processes. The time progress of monomer (m) conversion from the dispersed to aggregated state can then be followed by solving the following two kinetic equations for principal moments

$$\frac{dP(t)}{dt} = k_n m(t)^{n_c} + k_2 m(t)^{n_2} M(t) \quad (1)$$

$$\frac{dM(t)}{dt} = k_+ m(t) P(t) \quad (2)$$

where $P(t)$, $M(t)$, and $m(t)$ are the concentrations of supramolecular polymers, polymerized monomers, and monomers in solution, at time t, respectively. k_n is the rate constant for the formation of the primary nucleus, k_+ is the fibril elongation rate constant, k_2 is the secondary nucleus formation rate constant, and n_c and n_2 denote the nucleus sizes of the primary and secondary nucleation processes.

We note that although a nucleus is usually conceived as an aggregate, it is not necessarily the case for macromolecular monomers such as polypeptides. Nucleation is indeed used to identify the rate-limiting step in the formation of fibrils, and in some cases, a nucleus can even be "monomeric" if the refolding process of polypeptides rather than the oligomerization is rate-limiting. This refolding here refers to the conformational change of a monomer to an assembly-competent structure that is less stable than the original conformation but progressively more stable when assembled into larger aggregates.[65] The phenomenon was first discovered in polyglutamine assembly and thought to also exist in other amyloid fibrillations.[66] The concept is particularly relevant to particle-based nucleation, as a suitable particle surface may interact with polypeptides in

https://doi.org/10.1021/acs.biomac.1c01230
Biomacromolecules XXXX, XXX, XXX−XXX

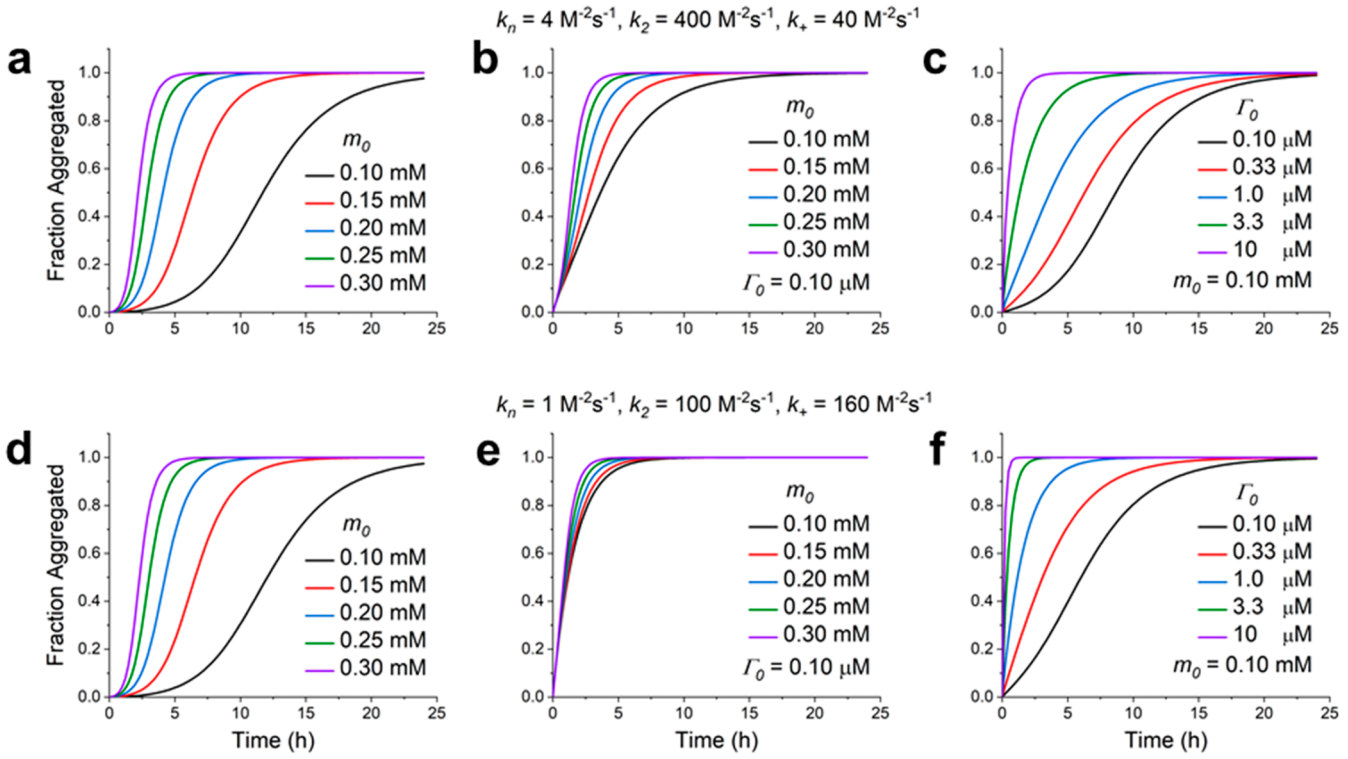

Figure 2. Simulations with the particle-regulated amyloid fibrillation model. (a–c) Plots of the fraction aggregated vs time for test cases with k_n = 4 M^{-2} s^{-1}, k_2 = 400 M^{-2} s^{-1}, and k_+ = 40 M^{-1} s^{-1} at selected values of m_0 and Γ_0. (d–f) Plots of the fraction aggregated vs time for test cases with k_n = 1 M^{-2} s^{-1}, k_2 = 100 M^{-2} s^{-1}, and k_+ = 160 M^{-1} s^{-1} at selected values of m_0 and Γ_0. Fraction aggregated was calculated using the numerical solutions of eqs 4–6. n_c = 3, n_2 = 2, k_f = 1 s^{-1}, and K_D = 1 μM.

such a way that the assembly-competent structure may subsequently be facilitated following the reversible binding of solution monomers on the surface, that is, similar to a two-step, Michaelis–Menten-like process commonly found in enzymatic reactions (the "enzyme" being a surface site).

Therefore, for particle-catalyzed amyloid fibrillation, the simplest possible mechanism may follow the principle of the Langmuir/Michaelis–Menten model, which is often used to explain how surfaces that bind reactants can activate them in some way for catalyzing reactions (Figure 1b). As there is no bond-breaking or bond-forming reactions in the amyloid fibrillation, the most plausible mechanism by which binding to a surface increases the rate of nucleation process is that surface interaction helps to pull the conformation of polypeptides (either helices or coils) into a structure resembling that in the nucleus (a "strain" mechanism), such as forming turns or chain reversals that can stack into antiparallel β-sheets. Suppose S is such a surface site that catalyzes the nucleation, the binding of a monomer (m) to the surface causes a conformational change that "activates" m, making it more "nucleus"-like; we can consider the reaction in two steps

$$m + S \underset{K_D}{\rightleftarrows} m{\cdot}S \xrightarrow{k_f} m^*{\cdot}S$$

Step 1 is the reversible adsorption of m to the surface to reach an activated state of $m{\cdot}S$. We use the Langmuir model for this step, where K_D is the dissociation equilibrium constant. Step 2 involves the conversion of the bound monomer to a nucleus-like conformation and assembly-ready, so that another incoming monomer may stack onto it and enter the propagation process. The second step involves crossing an energy barrier, which occurs with the rate constant k_f. The overall rate r of the production of nuclei on the surface is given by eq 3.

$$r = k_f\Gamma_0\theta = \frac{k_f\Gamma_0}{1 + K_D/m} \quad (3)$$

where Γ_0 is the concentration of the total binding sites, and θ is the fraction of surface that is covered by bound monomers.

Adding this particle-induced heterogeneous nucleation pathway into the existing model (eqs 1 and 2), and considering that the nuclei formed on the particle surface likely remain bound rather than being released into the solution, the kinetic equations for the principal moments then become

$$\frac{dP(t)}{dt} = k_n m(t)^{n_c} + k_2 m(t)^{n_2} M(t) \quad (4)$$

$$\frac{dP'(t)}{dt} = \frac{k_f\Gamma}{1 + K_D/m(t)} \quad (5)$$

$$\frac{dM(t)}{dt} = k_+ m(t)(P(t) + P'(t)) \quad (6)$$

where $P'(t)$ is concentration of fibrils initiated from the particle surface, and Γ is the concentration of binding sites on NPs, which are considered nonrecoverable once a fibril grows from it. Γ has an initial value of Γ_0 and decreases with time in the reaction. In the unlikely case that the binding sites can be fully recovered after the formation of nuclei (e.g., mature nuclei dissociate instantly from the site—a truly enzyme-like behavior), Γ would remain unchanged from its initial value, and this would lead to a very fast nucleation process that is

https://doi.org/10.1021/acs.biomac.1c01230
Biomacromolecules XXXX, XXX, XXX–XXX

rarely observed in artificial systems. As the binding affinity and the concentration of total binding sites can be experimentally determined from the binding isotherm, the fitting parameters in a typical kinetic analysis are the rate constants k_n,k_2, k_+, and k_f. It is a standard practice to determine the numerical solutions of these kinetic equations. When there are no catalytic particles in solution, eqs 4−6 reduce to eqs 1 and 2.

If the heterogeneous nucleation process does require multiple monomers on the surface (n') to form a nucleus, then the Hill equation can replace the Langmuir equation to account for the process, and the rate of the nucleation process on particles is given by eq 7 as

$$n'm + S \underset{K_D}{\rightleftarrows} m_n \cdot S \xrightarrow{k_f} m_n^* \cdot S$$

$$\frac{dP'(t)}{dt} = \frac{k_f \Gamma}{1 + (K_D/m(t))^{n'}} \quad (7)$$

In practice, unless n' is a large number (e.g., >3) and cooperative binding of a monomer on the particle surface is clearly evidenced in the experiments, the Langmuir equation is usually sufficient for calculating the occupancy of binding sites in the differential equations of the rate laws.

Simulations with the Particle-Regulated Amyloid Assembly Model

Figure 2 shows an example of the kinetics of assembly behavior at various initial concentrations of monomers (m_0), in the absence (Figure 2a,d) or presence (Figure 2b,c,e,f) of particle-based nucleators, predicted by eqs 4−6. n_c and n_2 were chosen to be 3 and 2, respectively, which are common values found in amyloid-like fibrillation. Without particles, the spontaneous formation of nuclei is the rate-limiting process in the initial stage (Figure 2a). Once some nuclei form and grow into fibrils, the secondary process starts to take control, and the rate of fibrillation accelerates. The rate of polymerization in the very early stage shows a clear power law dependence on m_0. It is also obvious that, in the absence of the $P'(t)$ term, the rate constants are contained in the form of product of k_+k_n and k_+k_2 in eqs 4 and 6. Therefore, kinetic analysis on the data in the absence of particles provides information as to the size of the nuclei for the primary and secondary processes and k_+k_n and k_+k_2 only. In the presence of particles, the formation of nuclei is now catalyzed by the particle surface, that is, a heterogeneous primary nucleation pathway, and individual rate constants can now be deconvoluted in eqs 4−6. The characteristic of particle-catalyzed polymerization is that the rate of polymerization in the initial stage loses dependence on m_0 and becomes approximately proportional to the concentration of particle nucleators (Figure 2b,c). As the binding isotherm between the monomer and particles can be easily measured experimentally, global analysis on a series of kinetic data from varying monomer and particle concentrations can determine the individual rate constants and lower limit of k_f with a good fidelity (see the Supporting Information for a MATLAB script on solving eqs 4−6 numerically).

The kinetic profiles in the presence of regulated particles are sensitive to the individual rate constants. Figure 2d−f shows the kinetic profiles simulated with k_+ that is 4 times larger than that in Figure 2a−c, while k_n and k_2 are 4 times smaller. As both k_+k_n and k_+k_2 remain the same, the kinetic profiles in the absence of particles (Figure 2d) are identical to that of Figure 2a. In the presence of catalytic particles, however, the kinetic profiles in Figure 2e,f are distinct from those of Figure 2b,c, respectively, as the fibril growth from the particle-regulated heterogeneous pathway is in control. Therefore, even with limited data sets, k_n, k_+, and k_2 can be determined with good accuracy (see an example of MATLAB script in the Supporting Information). On the other hand, determining K_D directly from the kinetic profiles is possible but would require data collected from various m_0 in the presence of particles, especially from the concentration range that is comparable to K_D. For the monomers with the modest to strong binding affinity to particles (e.g., K_D in the range of μM), it may not always be practical. Additionally, k_f cannot be determined without knowing the Γ_0 first (k_f and Γ appear as products in the rate equations). Therefore, in practice, measuring K_D and Γ_0 is a prerequisite for applying the model to analyze the particle-regulated assembly kinetics of synthetic polypeptides. Next, we show the use of this model in designing and analyzing the particle-regulated fibrillation of PLGs in aqueous solution.

Amyloid-like Assembly of PLGs

PLGs and other ionic homopeptides have predictable conformational structures, and their interactions can be modulated in solution.[18] The aggregation behaviors of PLGs in aqueous solution are nucleation-controlled processes and show interesting structures at different hierarchical levels, from nanosized amyloid fibrils and their twisted, bowtie-like bundles to micron-sized, spherulitic assemblies.[20] Additionally, block or random copolymers of PLGs can readily be synthesized to tune their interactions in aqueous solution. Therefore, we chose PLGs as our supramolecular monomers to test the model for the regulated assembly of synthetic polypeptides. PLGs with low polydispersity ($Đ$ < 1.1) were synthesized by the controlled ring-opening polymerization of amino acid NCA (see the Materials and Methods section and Figures S1 2 for the synthesis and characterization).[59,60] Figure S3 shows the conformations of PLG_{50} (DP ∼ 50) at different pHs, as examined by CD. At pH 4, PLG_{50} is dispersed as α-helices in a freshly made solution (15 mM sodium acetate buffer), but slowly associated into amyloid fibrils that further aggregate into twisted ribbons at temperatures above 30 °C (Figure 3a,b), and eventually into spherulitic assemblies after incubation for over 40 h (Figure 3c), similar to previous reports.[20] The β-sheet structure in mature PLG_{50} fibrils was confirmed by the FTIR analysis (Figure S4a), and the superstructure of the large spherulitic aggregates can be visualized by fluorescence microscopy (Figure 3d) after staining the sample with ThT, a fluorescent probe which shows a large fluorescence enhancement upon binding to the cross-β-amyloid fibrils.[67] The formation of spherulitic amyloid superstructures (size distribution shown in Figure S4b) from PLG fibrils is similar to the formation of spherulites by the amyloid fibrils of bovine insulin, the mechanism of which was previously discussed.[68,69]

Upon introduction of cationic silica NPCs into the solution, anionic PLGs bind to the particle surface, reducing the repulsive interactions between PLGs and increasing the likelihood of refolding and stacking of local PLGs to form amyloid-like fibrils. Cationic NPCs were prepared by surface modification of silica NPs (∼20 nm in diameter) with APTES, following established methods (see the Materials and Methods section and Figure S5 for the synthesis and characterizations).[70] The silica NPCs are composed of multiple NPs of 20 nm in diameter, have an average size of 130 nm as measured by DLS (Figure S5c−g), and have a zeta potential of

https://doi.org/10.1021/acs.biomac.1c01230
Biomacromolecules XXXX, XXX, XXX−XXX

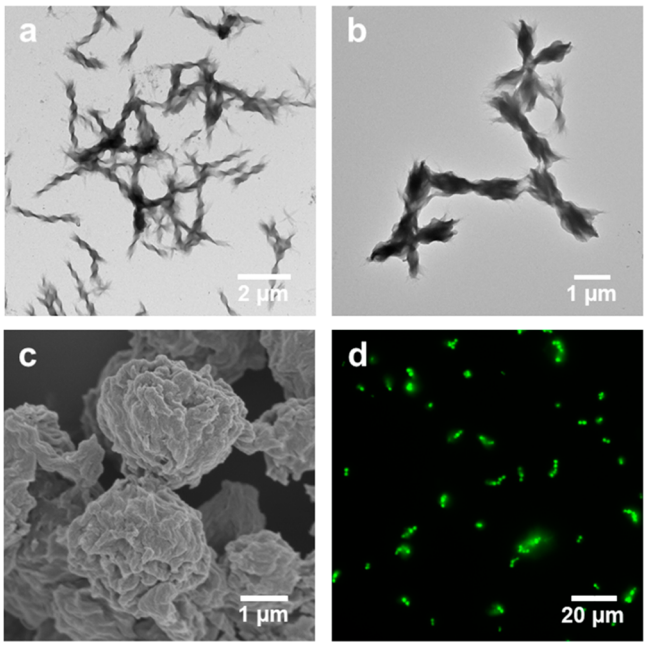

Figure 3. Hierarchically organized structures assembled from PLG_{50} in aqueous solution ($[PLG_{50}]$ = 0.13 mM) at 45 °C. TEM images of fibrils and fibril bundles formed in solution after incubation for (a) 10 and (b) 20 h. (c) SEM image of large spherite superstructures formed from further bundling of fibrils in solution after incubation for 40 h. (d) Fluorescence microscopy image of the superstructure in (c) after staining with 50 μM of ThT.

+34.4 mV in 15 mM sodium acetate at pH 4.0. The use of NPCs formed by small NPs increases the surface area-to-volume ratio[71] and makes it easy to separate NPCs by centrifugation. The binding isotherms between the NPCs and PLG_{50} in the solution were carefully measured at different temperatures and fitted by the Langmuir equation (Figures 4 and S6). The K_D value of PLG_{50} to the surface of cationic NPCs was 1.3 μM at 45 °C and 2.6 μM at 75 °C. τ_0, the binding capacity, was found to be 81 μmol/g NPC at 45 °C and 141 μmol/g NPC at 75 °C. Clearly, PLGs can bind tightly to cationic NPCs through electrostatic interactions, and increasing the temperature only modestly reduced the binding affinity. Introduction of NPCs into the solution of PLGs drastically accelerated the assembly process at 45 and at 75 °C. The morphologies of the resulting supramolecular structures at different hierarchical levels (Figure S7) are similar to those in Figure 3, although the spherulitic assemblies tend to further aggregate into networks, as evidenced in the fluorescence microscopy images.

Kinetics of the Polypeptide Assembly and Fitting of Assembly Kinetics with the Model

The assembly of PLGs in the absence and presence of NPCs by ThT fluorescence, which can be used to quantify amyloid fibrils formed in the solution at a given time interval, is a common method to track the growth of amyloid-like aggregates from polypeptides. ThT can quickly bind to an amyloid-like structure in solution, and the fluorescence of bound ThT varies linearly with the mass concentration of fibrils, as demonstrated by many groups[64,72] as well as our own experiments (Figure S8). We used an "ex situ" ThT fluorescence measurement instead of an "in situ" method which has ThT present in the solution for continuous monitoring of the assembly process. This is to minimize the interference of ThT on the nucleation process, as ThT has a positive charge and may act as a molecular cofactor.

Figure 5a,b shows the assembly kinetics of PLG_{50} into fibrils at pH 4 and at 45 or 75 °C at different initial concentrations of PLG_{50}. As in previous studies, the PLG assembly occurred in two distinct stages, with a slow nucleation step followed by a faster fibril growth. Increasing the concentration of PLG reduced the time required to enter the growth stage, suggesting that the spontaneous formation of nuclei in solution requires the interaction of a few PLG chains. Thus, a higher concentration of PLG increases the likelihood of formation of oligomeric nuclei. Figure S9 shows the global fit of kinetic profiles at each temperature by solving the differential rate equations (eqs 1 and 2) numerically. n_c and n_2 were determined to be 3 and 2 at both temperatures. We note that these values are related to the effective portion of the nucleating aggregate that participates in the conformational conversion rather than the overall size of the nucleating aggregates. The slow nucleation is presumably due to the repulsive interactions of charged PLG monomers and the activation barrier in unfolding the α-helical PLGs to permit stable stacking into the β-sheet structure. k_+k_n and k_+k_2 were determined to be 57 ± 6 and 6280 ± 380 M^{-3} s^{-2} at 45 °C and

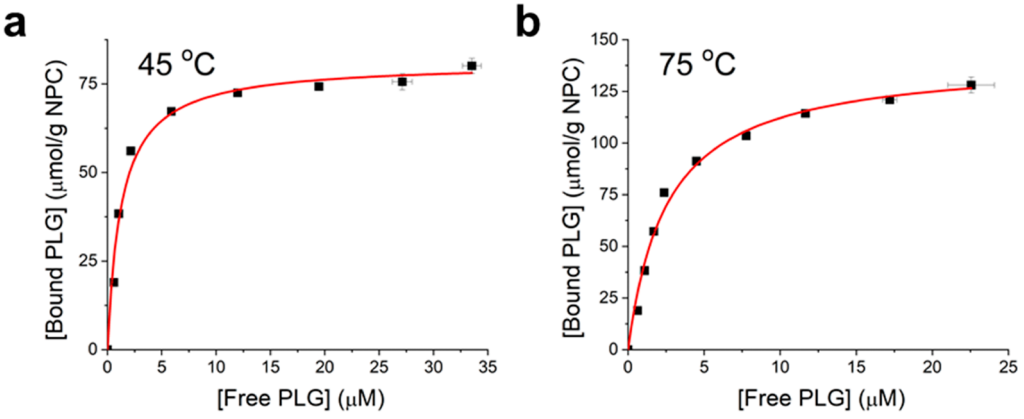

Figure 4. Adsorption of PLG_{50} on cationic NPCs. Adsorption isotherms of PLG_{50} on cationic NPCs at (a) 45 and (b) 75 °C. The NPC concentration was kept constant (at 0.4 mg/mL) with the increase of the PLG_{50} concentration from 0 to 75 μM. The data (black squares) were fit with the Langmuir adsorption model (red lines) to obtain the binding affinity and binding capacity of PLG_{50} on cationic NPCs.

https://doi.org/10.1021/acs.biomac.1c01230
Biomacromolecules XXXX, XXX, XXX−XXX

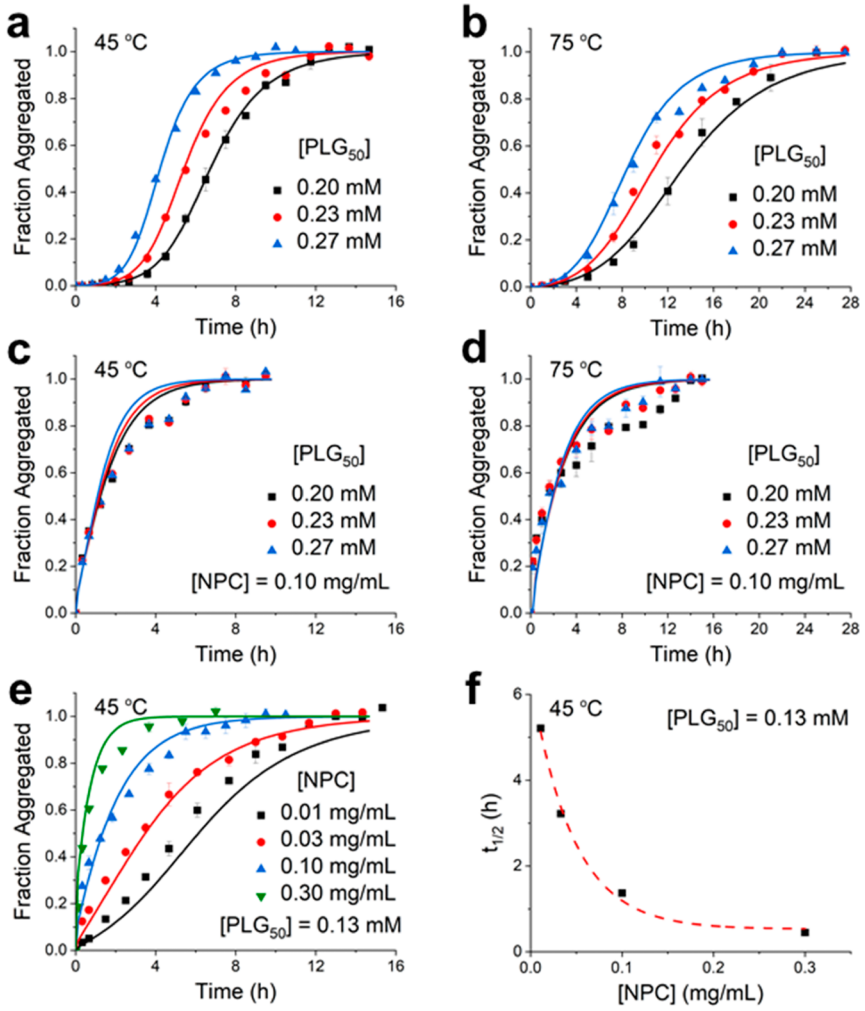

Figure 5. Analysis of the supramolecular assembly of PLG_{50} in the absence and presence of cationic NPCs with the kinetic model. Assembly kinetics of PLG_{50} (0.2−0.27 mM) at 45 (a) and 75 °C (b), PLG_{50} (0.2−0.27 mM) in the presence of 0.1 mg/mL cationic NPCs (Γ_0 = 8.1 μM) at 45 (c) and 75 °C (d), and PLG_{50} (0.13 mM) regulated by increasing concentrations of NPC (Γ_0 = 0.8, 2.4, 8.1, and 24.3 μM, respectively) (e) and fit with the kinetic model (eqs 4−6) by sharing the same kinetic rate constants for all the kinetic profiles collected at the same temperature (Table 1). (f) Plot of the half-assembly time, $t_{1/2}$, against [NPC] in (e); the dashed line is provided for visual guidance. Data are representative of three replicate experiments.

39 ± 8 and 837 ± 85 M^{-3} s^{-2} at 75 °C, respectively. As we mentioned earlier, it is their product rather than individual rate constants which can be determined in the absence of NPCs.

In marked contrast, the introduction of even small amounts of cationic NPCs (0.1 mg/mL) eliminated the slow lag phase (Figure 5c,d), drastically reducing the time required to complete the assembly process. When catalyzed by NPCs, the time progress of amyloid formation became independent of initial PLG concentrations. Varying the NPC concentration efficiently regulated the apparent kinetic rates (Figure 5e), demonstrating the effectiveness of NPCs as a primitive nucleation factor. The half-life of polymerization time, $t_{1/2}$ (time taken to reach 50% of the equilibrium fibril mass) reduced more than 10-fold from 5.3 to 0.3 h at 45 °C, when [NPC] increased from 0.01 to 0.3 mg/mL (Figure 5f). Negatively charged NPs, such as poly(acrylic acid)-coated gold NPs (PAA−AuNPs)[73] (see the Supporting Information for the synthesis, Figure S10a), and neutral NPs, such as poly(*N*,*N*-dimethylacrylamide)-coated gold NPs (PDMA−AuNPs) (see the Supporting Information for the synthesis, Figure S10b), did not accelerate the PLG assembly, as confirmed in our control experiments (Figure S11).

The nucleator-like effect of cationic NPCs and accelerated PLG assembly is clearly evidenced. The accumulation of PLG_{50} onto particle surface facilitated the rapid nucleation and growth of amyloid fibrils. The insensitivity of the kinetic profiles to the PLG concentration indicates a low reaction order with respect to monomers, in contrast to multiple monomers (n_c = 3) required in primary nucleation in the absence of NPCs, similar to what was predicted by our model. The strong dependence of polymerization rates on [NPC] suggests that the particle surface acts like a one-time-use catalyst for PLG nucleation. Presumably, the attractive electrostatic interactions between the NPCs and PLGs facilitate the conformational change of helical chains to structures resembling the nucleus, permitting the incoming PLGs to further stack on them to form a stable β-sheet structure. We applied the kinetic model described in the previous section to analyze the data quantitatively.

The simple kinetic model (Figure 1 and eqs 4−6) can fit all the kinetic profiles collected (both in the absence and presence

https://doi.org/10.1021/acs.biomac.1c01230
Biomacromolecules XXXX, XXX, XXX−XXX

of NPCs) at a given temperature simultaneously, without any fudge factors. The colored lines in Figure 5a–e show the calculated kinetic curves from solving eqs 4–6 numerically, where the rate constants are shared by all curves at a given temperature (Table 1). The experimentally measured values of

Table 1. Rate Constants Obtained from the Global Analysis of PLG Assembly Kinetics from Figure 5

	k_n (M^{-2} s^{-1})	k_+ (M^{-1} s^{-1})	k_2 (M^{-2} s^{-1})	k_f (s^{-1})
45 °C	2.1 ± 0.3	15 ± 1	480 ± 35	>0.9
75 °C	4.8 ± 0.8	6.4 ± 0.4	134 ± 20	>0.2

K_D and Γ_0 at each temperature were directly used in the equation. k_f was determined to have a value in the order of 0.9 s^{-1} at 45 °C and 0.2 s^{-1} at 75 °C. This provides a sense on the rearrangement time required for surface-bound PLGs to form pseudonuclei, on which incoming PLGs can stack and form a β-sheet structure. The model successfully describes the concentration dependence of the kinetic curves on m_0 in the absence of NPCs and the catalytic behavior of NPC nucleators under varying m_0 and NPC concentrations.

Critical Role of the Refolding Process Facilitated by Particle–Polypeptide Interaction

To confirm that the NPC surface can instantaneously provide a heterogeneous nucleation pathway, we monitored the early stage of assembly process by CD. Figure 6 compares the time-dependent CD spectra of PLG_{50} in the absence and presence of NPCs. At time 0, PLGs showed a strong negative signal at 222 and 208 nm, which are the characteristic peaks of α-helix. Signals from the β-sheet PLG amyloid fibrils are much weaker, with a minimum at 216 nm, and easily obscured in the aggregates.[74] Without NPCs, the CD signals remained to be the same for the first few hours (Figure 6c), due to the slow nucleation stage. In contrast, the signals started to diminish as soon as NPCs were added (Figure 6c), suggesting that the refolding of the bound PLGs into the pseudonucleus and the formation of β-sheet amyloid fibrils occurred rapidly on the particle surface. A similar study on PLG_{85} gave an identical result (Figure S12).

Additional control experiments were carried out to elucidate the requirements in designing particle-based nucleation factors. First, binding between the polypeptides and particles is a prerequisite, but it is not sufficient. As an example, PLG assembly at pH 4 occurs extremely slow at room temperature (25 °C), beyond our detection window (48 h). PLG binds tightly to cationic NPCs at room temperature (Figure S13), but the NPCs alone cannot accelerate the assembly process at this temperature, and the CD signals showed no change in the presence of NPCs (Figure S14). Only at elevated temperatures, the particle-bound PLGs can overcome the activation energy required for nucleus formation. Second, the particle may not further accelerate the fibrillation if the spontaneous primary nucleation process is not the rate-limiting process, for example, being extremely fast in the experimental conditions or through "monomeric nuclei" ($n_c \sim 1$). To investigate this, we tested the amyloid fibrillation of PLL in the presence of anionic NPs such as PAA–AuNPs. Long-chain PLLs (DP > 200), which are thought to form a series of turns and chain reversals in basic solution at elevated temperatures,[75] required relatively low activation energy to organize into long fibrils of antiparallel β-sheets (Figure S15a,b) in the aggregation process. Figure 7 compares the time progress of CD signals of PLL_{298} with and without anionic PAA–AuNPs. The strong binding affinity of PLL on PAA–AuNPs was obvious based on their equilibrium-binding isotherm (Figure S15c). However, PAA–AuNPs did not accelerate the supramolecular assembly of PLL_{298}. The kinetics were nearly identical, whether the particles were present or absent (Figure 7c). This is because the nucleation process for long PLL does not require an oligomerization step, as a helical PLL chain with sufficient length consists of a "broken-rod" structure that turns into a β-sheet relatively easily. In other words, PLL can assemble rapidly at elevated temperatures, with no significant lag phase from the nucleation step. In this case, particles cannot facilitate any rate acceleration.

Combining all these results, it appears to us that the formation of surface-induced nuclei in the polypeptide assembly process may consist of at least two steps: the binding of polypeptide chains to the particle surface and a subsequent conformational change of the adsorbed polypeptide to form a nucleus for fibril growth. While it is a surface-facilitated phenomenon, the rate equation shows some similarity with a Michaelis–Menten-like equation, which is well established to describe the catalytic reactions of many enzymes or enzyme-like systems. Once the fibrils form on the particle surface, they can also serve as secondary nucleation sites, as in the case of solution kinetics. The combined effect leads to the accelerated

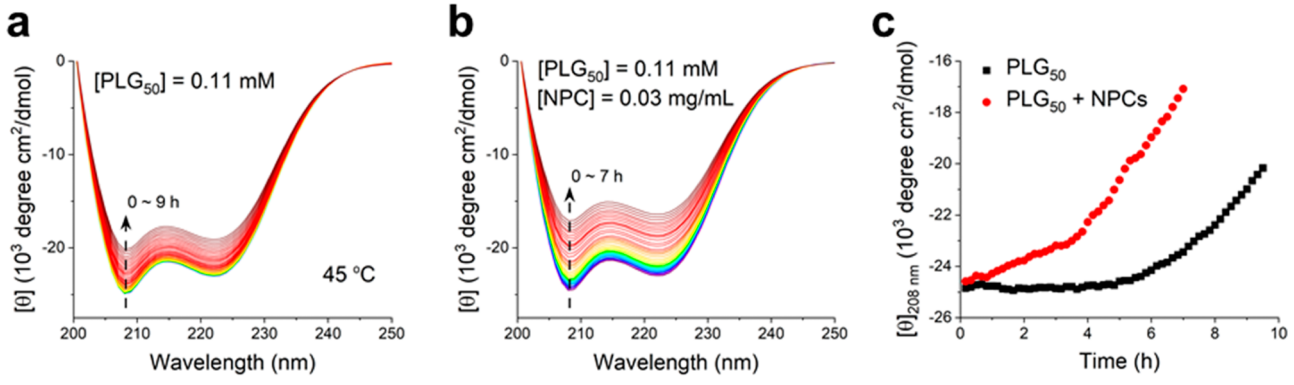

Figure 6. Comparison of the early assembly kinetics and conformational change of PLG_{50} at 45 °C in the absence and presence of cationic NPCs, as monitored by CD spectroscopy. Time progress of CD signals from the PLG_{50} solution (0.11 mM) in the absence (a) and in the presence (b) of 0.03 mg/mL of NPCs (Γ_0 = 2.4 μM). The rainbow-like colors were used to provide a visual guidance of the time progress. (c) Plot of early assembly kinetics based on the time-dependent CD signals at 208 nm in (a, b).

https://doi.org/10.1021/acs.biomac.1c01230
Biomacromolecules XXXX, XXX, XXX–XXX

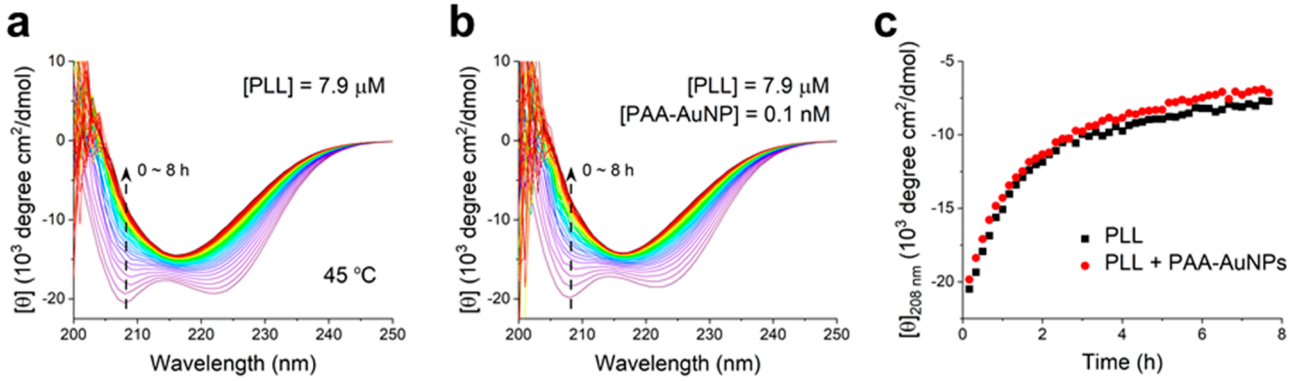

Figure 7. Comparison of early assembly kinetics and conformational change of PLL_{298} at 45 °C in the absence and presence of anionic PAA–AuNPs, as monitored by CD spectroscopy. Time progress of CD signals from PLL_{298} solution (7.9 μM) in the absence (a) and in the presence (b) of PAA–AuNPs (0.1 nM). The rainbow-like colors were used to provide a visual guidance of the time progress. (c) Plot of early assembly kinetics based on the time-dependent CD signals at 208 nm in (a, b).

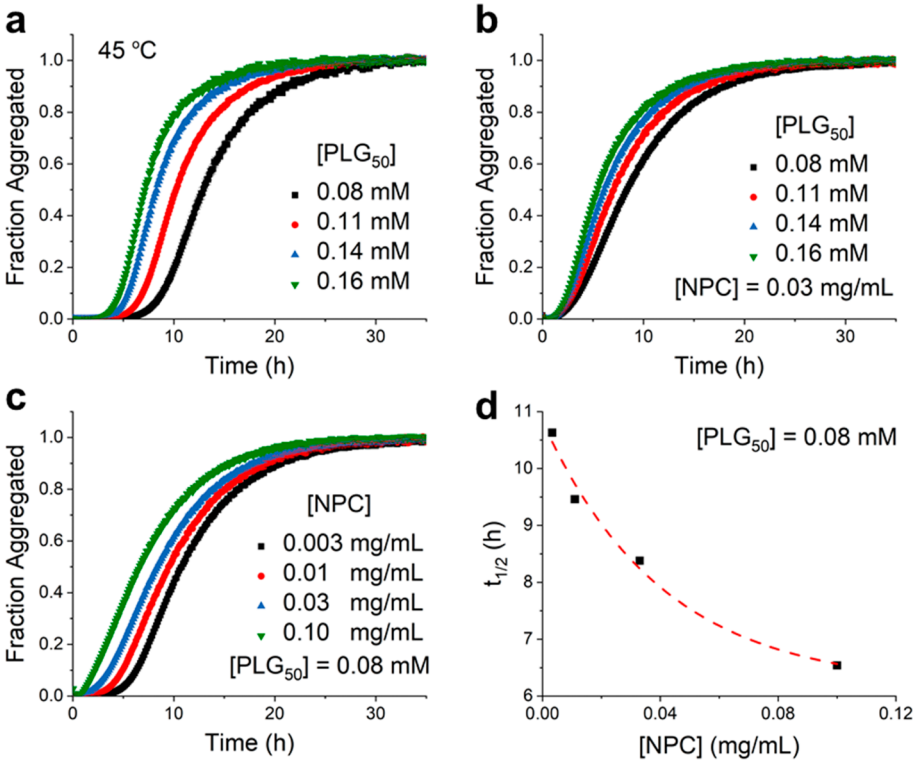

Figure 8. Assembly kinetics of PLG_{50} in the absence and in the presence of cationic NPCs, as monitored by in situ ThT fluorescence measurements. Assembly kinetics of PLG_{50} (0.08–0.16 mM) at 45 °C (a), PLG_{50} (0.08–0.16 mM) in the presence of 0.03 mg/mL cationic NPCs (Γ_0 = 2.4 μM) at 45 °C (b), and PLG_{50} (0.08 mM) regulated by increasing concentrations of NPC (Γ_0 = 0.2, 0.8, 2.4, and 8.1 μM) (c). Data are representative of three replicate experiments. The error bars are smaller than the size of symbols. (d) Plot of the half-assembly time, $t_{1/2}$, against [NPC] in (c); the dashed line is provided for visual guidance.

assembly of polypeptides into amyloid fibrils, which can further bundle together or form a cross-linked network or superstructures afterward, as the nucleation of new fibrils on the existing ones generates attached arrays or webs of fibrils. Thus, particles can catalyze a heterogeneous primary nucleation pathway that is much faster than the corresponding steps in solution.

Other Molecular Factors Affecting the Assembly

We also note that nucleators are not the only molecular factors that may affect the assembly of synthetic polypeptides in aqueous solution. Specific ions or molecules may also act as rate regulators to accelerate or decelerate the kinetic process by complexing with the polypeptide chain and making its conformational structure more favorable or less favorable for assembly. We have mentioned the reason why we avoided the use of in situ fluorescence experiments for the kinetic study: dispersed ThT molecules or their micelles in the solution may bind to PLGs or fibrils and affect the kinetics.[76,77] Figure 8 shows the kinetic profiles of the PLG assembly without or with NPCs at 45 °C, from in situ ThT fluorescence measurements. Using an automated microplate reader, the continuous development of kinetic profiles was collected with superior quality and reproducibility. However, the presence of ThT in the solution changed the apparent reaction order of primary

https://doi.org/10.1021/acs.biomac.1c01230
Biomacromolecules XXXX, XXX, XXX–XXX

nucleation with respect to the PLG concentrations ($n_c \sim 2$) (Figure S16). Nevertheless, the general trend of kinetic profiles under particle regulation still agreed with the predictions of our model (e.g., the simulated profiles in Figure 2). The full description of the kinetic behavior under the coexistence of a potential secondary molecular cofactor requires the consideration of its binding equilibrium with polypeptides at different conformational states, which were discussed as "p (parameter) molecules" by Oosawa in his classic book on supramolecular polymerization of proteins. The refinement of the kinetic model to reflect the potential influence of additional molecular cofactors is the subject of future study.

Potential Limitations of Particle-Based Regulators

In the end, we discuss the potential limitations of current particle-based regulators and make suggestions on what need to be overcome to develop more sophisticated synthetic nucleators. First, like an enzyme, a true nucleation factor should be able to release the mature nuclei and regenerate the active sites to continue the catalytic process. For this purpose, there should be an optimal binding affinity for catalytic effectiveness in nucleators. If monomers bind to the nucleators too weakly, the reaction is slow because there is little "reactant" on the surface. When a monomer binds the nucleator too strongly, the reaction is also slow because the "product" (nucleus) is slow to leave the surface, occupying the sites where new monomers could bind. The best nucleators should bind neither too weakly nor too strongly. However, it is difficult to design particle-based regulators to have relatively high affinity for the transition state of the reaction that also do not bind monomers too weakly or nuclei too tightly. In this context, a macromolecule-based regulator, with the size, architecture, and binding affinity similar to the biological nucleators such as Arp2/3 and formins, may be a promising candidate, as the conformational change of complex macromolecules may be used to engineering dynamic binding properties desired for a more sophisticated nucleation factor. Second, for the purpose of quantitative analysis and predicting the regulated kinetics, the binding affinity and maximal binding sites on particles need to be measured accurately. This may be challenging in some cases, when the binding isotherm deviates from the Langmuir isotherm (e.g., a cooperative binding). In the model-based analysis, any inaccuracy in determining the binding sites would directly propagate into the value of rate constants. Third, a question that remains to be answered is related to the surface diffusion of bound monomers on the particle surface, which is thought to accelerate the rate of nucleation, either by the increased local molarity of monomers or by the enhanced prospect of clustering in a confined space. In a preliminary test, a variation of the current model was found to account for the kinetic data at 45 °C, even better by considering a fast segregation of bound monomers on a particle surface (see the Supporting Information, eqs S3−S9). Figure S17 and Table S1 show the calculated kinetic curves and kinetic rate constants from solving these differential equations numerically, where the rate constants are shared by all curves. The improvement in the fit quality, however, is not sufficient to reach a firm conclusion, considering that new parameters were added into the equations.

CONCLUSIONS

We proposed a simple kinetic model to describe the particle-accelerated self-assembly of synthetic polypeptides in aqueous solution and demonstrated an effective strategy to achieve such a behavior, in which cationic nucleators accelerated the nucleation and subsequent growth of anionic PLGs. The cationic particles serve to locally concentrate the PLG monomers on the surface and facilitate their conformational change required for stacking into amyloid-like fibrils. The primary heterogeneous nucleation pathway follows a Langmuir/Michaelis−Menten-type scheme. While we exclusively focused on homopolymers in this study, the preliminary result from the random copolymers of synthetic polypeptides (e.g., by including a second type of amino acids that have hydrophobic side chains) suggests that the abovementioned mechanism is equally applicable. The findings provide an exciting example and a theoretical framework of how artificial nucleators may be designed and refined further, based on macromolecular interactions and affinities. These efforts should offer an important insight into the rational design of next-generation artificial nucleators with higher complexity and greater regulatory control of supramolecular assembly in aqueous solutions.

ASSOCIATED CONTENT

Supporting Information

The Supporting Information is available free of charge at https://pubs.acs.org/doi/10.1021/acs.biomac.1c01230.

Additional experimental details on the synthesis of PAA−AuNPs and PDMA−AuNPs; additional methods for the calibration of the ThT fluorescence assays, analysis of the early-stage PLG assembly kinetics, and a variation of the surface-induced polymerization model; synthetic routes and GPC results of PLG and PLL polymers; pH-induced conformational changes in PLG by CD; FTIR-ATR results of PLG supramolecular assemblies; synthetic route and FTIR, DLS, TEM, and SEM results of NPCs; linear relationship between UV absorbance at 209 nm and the concentration of PLG_{50} α-helices; TEM and fluorescence microscopy images of PLG_{50} in the presence of NPCs; linear relationship between ThT fluorescence and mass concentration of PLG_{50} fibrils; global fit on the supramolecular assembly kinetics of PLG_{50} based on a nucleated polymerization model; TEM images of the polymer-grafted AuNPs; control experiments of supramolecular assembly kinetics in the presence of negatively charged and neutral NPs; early assembly kinetics and conformational change of PLG_{85} at 45 °C in the absence and presence of NPCs, as monitored by CD spectroscopy; adsorption isotherm of PLG_{50} on cationic NPCs at 25 °C; early assembly kinetics and conformational change of PLG_{50} at 25 °C in the presence of cationic NPCs, as monitored by CD spectroscopy; hierarchically organized structures assembled from PLL_{298} by TEM and adsorption isotherm of PLL_{298} on PAA−AuNPs; model-based analytical fit of PLG_{50} early-stage assembly at 45 °C by an in situ ThT approach; analysis of supramolecular assembly of PLG_{50} in the absence and presence of cationic NPCs with the variation model; and source code for kinetic simulations in Figure 2 and sample fittings (PDF)

AUTHOR INFORMATION

Corresponding Authors

Jianjun Cheng − *Department of Chemistry and Department of Materials Science and Engineering, University of Illinois at*

https://doi.org/10.1021/acs.biomac.1c01230
Biomacromolecules XXXX, XXX, XXX−XXX

Urbana-Champaign, Urbana, Illinois 61801, United States; orcid.org/0000-0003-2561-9291; Email: jianjunc@illinois.edu

Challa V. Kumar − *Department of Chemistry, University of Connecticut, Storrs, Connecticut 06269, United States;* orcid.org/0000-0002-4396-8738; Email: challa.kumar@uconn.edu

Yao Lin − *Polymer Program, Institute of Materials Science and Department of Chemistry, University of Connecticut, Storrs, Connecticut 06269, United States;* orcid.org/0000-0001-5227-2663; Email: yao.lin@uconn.edu

Authors

Tianjian Yang − *Polymer Program, Institute of Materials Science, University of Connecticut, Storrs, Connecticut 06269, United States*

Kyle Benson − *Department of Chemistry, University of Connecticut, Storrs, Connecticut 06269, United States;* orcid.org/0000-0001-9986-6696

Hailin Fu − *Department of Chemistry, University of Connecticut, Storrs, Connecticut 06269, United States;* orcid.org/0000-0002-3972-7659

Tianrui Xue − *Department of Chemistry, University of Illinois at Urbana-Champaign, Urbana, Illinois 61801, United States*

Ziyuan Song − *Department of Materials Science and Engineering, University of Illinois at Urbana-Champaign, Urbana, Illinois 61801, United States;* orcid.org/0000-0002-3165-3712

Hanyi Duan − *Polymer Program, Institute of Materials Science, University of Connecticut, Storrs, Connecticut 06269, United States*

Hongwei Xia − *Department of Chemistry, University of Connecticut, Storrs, Connecticut 06269, United States*

Ankarao Kalluri − *Department of Chemistry, University of Connecticut, Storrs, Connecticut 06269, United States*

Jie He − *Polymer Program, Institute of Materials Science and Department of Chemistry, University of Connecticut, Storrs, Connecticut 06269, United States;* orcid.org/0000-0003-0252-3094

Complete contact information is available at: https://pubs.acs.org/10.1021/acs.biomac.1c01230

Author Contributions

T.Y., K.B., and H.F. contributed equally. T.Y., K.B., H.F., T.X., J.H., J.C., C.V.K., and Y.L. conceived and designed the experiments. T.Y., K.B., T.X., Z.S. H.D., H.X., and A.K. performed the experiments. T.Y., K.B., H.F., T.X., Z.S., J.H., J.C., C.V.K., and Y.L. analyzed the data and prepared the manuscript with contributions from all authors.

Notes

The authors declare no competing financial interest.

■ ACKNOWLEDGMENTS

This work was supported by the NSF grant (DMR 1809497) and by the Graduate Assistance in Areas of National Need (GAANN) fellowship (Award P200A150330 and P200A180065). C.V.K. thanks the OVPR Research Excellence Award. The authors thank Joseph Gorecki for help with binding studies. The authors thank Prof. Carolyn Teschke for granting access to circular dichroism measurement (NIH 3R01GM076661-11S1) and Richard Whitehead for help with the instrument training.

■ REFERENCES

(1) Kang, J.; Miyajima, D.; Mori, T.; Inoue, Y.; Itoh, Y.; Aida, T. A rational strategy for the realization of chain-growth supramolecular polymerization. *Science* **2015**, *347*, 646−651.

(2) Korevaar, P. A.; George, S. J.; Markvoort, A. J.; Smulders, M. M. J.; Hilbers, P. A. J.; Schenning, A. P. H. J.; De Greef, T. F. A.; Meijer, E. W. Pathway complexity in supramolecular polymerization. *Nature* **2012**, *481*, 492−496.

(3) Zhang, W.; Jin, W.; Fukushima, T.; Saeki, A.; Seki, S.; Aida, T. Supramolecular linear heterojunction composed of graphite-like semiconducting nanotubular segments. *Science* **2011**, *334*, 340−343.

(4) Ogi, S.; Sugiyasu, K.; Manna, S.; Samitsu, S.; Takeuchi, M. Living supramolecular polymerization realized through a biomimetic approach. *Nat. Chem.* **2014**, *6*, 188−195.

(5) Ogi, S.; Stepanenko, V.; Thein, J.; Würthner, F. Impact of alkyl spacer length on aggregation pathways in kinetically controlled supramolecular polymerization. *J. Am. Chem. Soc.* **2016**, *138*, 670−678.

(6) Datta, S.; Kato, Y.; Higashiharaguchi, S.; Aratsu, K.; Isobe, A.; Saito, T.; Prabhu, D. D.; Kitamoto, Y.; Hollamby, M. J.; Smith, A. J.; Dalgliesh, R.; Mahmoudi, N.; Pesce, L.; Perego, C.; Pavan, G. M.; Yagai, S. Self-assembled poly-catenanes from supramolecular toroidal building blocks. *Nature* **2020**, *583*, 400−405.

(7) Boekhoven, J.; Hendriksen, W. E.; Koper, G. J. M.; Eelkema, R.; van Esch, J. H. Transient assembly of active materials fueled by a chemical reaction. *Science* **2015**, *349*, 1075−1079.

(8) Li, X.; Kuang, Y.; Lin, H.-C.; Gao, Y.; Shi, J.; Xu, B. Supramolecular nanofibers and hydrogels of nucleopeptides. *Angew. Chem., Int. Ed.* **2011**, *50*, 9365−9369.

(9) Yu, Z.; Tantakitti, F.; Yu, T.; Palmer, L. C.; Schatz, G. C.; Stupp, S. I. Simultaneous covalent and noncovalent hybrid polymerizations. *Science* **2016**, *351*, 497−502.

(10) Besenius, P.; Portale, G.; Bomans, P. H. H.; Janssen, H. M.; Palmans, A. R. A.; Meijer, E. W. Controlling the growth and shape of chiral supramolecular polymers in water. *Proc. Natl. Acad. Sci. U.S.A.* **2010**, *107*, 17888−17893.

(11) Sorrenti, A.; Leira-Iglesias, J.; Sato, A.; Hermans, T. M. Non-equilibrium steady states in supramolecular polymerization. *Nat. Commun.* **2017**, *8*, 15899.

(12) Aida, T.; Meijer, E. W. Supramolecular Polymers—we've Come Full Circle. *Isr. J. Chem.* **2020**, *60*, 33−47.

(13) Oosawa, F.; Asakura, S. *Thermodynamics of the Polymerization of Protein*; Academic Press, 1975.

(14) Oosawa, F.; Kasai, M. A theory of linear and helical aggregations of macromolecules. *J. Mol. Biol.* **1962**, *4*, 10−21.

(15) Zhao, D.; Moore, J. S. Nucleation-elongation: a mechanism for cooperative supramolecular polymerization. *Org. Biomol. Chem.* **2003**, *1*, 3471−3491.

(16) De Greef, T. F. A.; Smulders, M. M. J.; Wolffs, M.; Schenning, A. P. H. J.; Sijbesma, R. P.; Meijer, E. W. Supramolecular polymerization. *Chem. Rev.* **2009**, *109*, 5687−5754.

(17) Gillam, J. E.; MacPhee, C. E. Modelling amyloid fibril formation kinetics: mechanisms of nucleation and growth. *J. Phys.: Condens. Matter* **2013**, *25*, 373101.

(18) Fändrich, M.; Dobson, C. M. The behaviour of polyamino acids reveals an inverse side chain effect in amyloid structure formation. *EMBO J.* **2002**, *21*, 5682−5690.

(19) Aggeli, A.; Nyrkova, I. A.; Bell, M.; Harding, R.; Carrick, L.; McLeish, T. C. B.; Semenov, A. N.; Boden, N. Hierarchical self-assembly of chiral rod-like molecules as a model for peptide-sheet tapes, ribbons, fibrils, and fibers. *Proc. Natl. Acad. Sci. U.S.A.* **2001**, *98*, 11857−11862.

(20) Colaco, M.; Park, J.; Blanch, H. The kinetics of aggregation of poly-glutamic acid based polypeptides. *Biophys. Chem.* **2008**, *136*, 74−86.

(21) Lashuel, H. A.; LaBrenz, S. R.; Woo, L.; Serpell, L. C.; Kelly, J. W. Protofilaments, filaments, ribbons, and fibrils from peptidomimetic self-assembly: implications for amyloid fibril formation and materials science. *J. Am. Chem. Soc.* **2000**, *122*, 5262−5277.
(22) Wang, J.; Lu, H.; Kamat, R.; Pingali, S. V.; Urban, V. S.; Cheng, J.; Lin, Y. Supramolecular polymerization from polypeptide-grafted comb polymers. *J. Am. Chem. Soc.* **2011**, *133*, 12906−12909.
(23) Won, Y.-Y.; Davis, H. T.; Bates, F. S. Giant wormlike rubber micelles. *Science* **1999**, *283*, 960−963.
(24) Su, H.; Zhang, W.; Wang, H.; Wang, F.; Cui, H. Paclitaxel-promoted supramolecular polymerization of peptide conjugates. *J. Am. Chem. Soc.* **2019**, *141*, 11997−12004.
(25) Warren, N. J.; Armes, S. P. Polymerization-induced self-assembly of block copolymer nano-objects via RAFT aqueous dispersion polymerization. *J. Am. Chem. Soc.* **2014**, *136*, 10174−10185.
(26) Fenyves, R.; Schmutz, M.; Horner, I. J.; Bright, F. V.; Rzayev, J. Aqueous self-assembly of giant bottlebrush block copolymer surfactants as shape-tunable building blocks. *J. Am. Chem. Soc.* **2014**, *136*, 7762−7770.
(27) Fernandez-Castano Romera, M.; Lafleur, R. P.; Guibert, C.; Voets, I. K.; Storm, C.; Sijbesma, R. P. Strain stiffening hydrogels through self-assembly and covalent fixation of semi-flexible fibers. *Angew. Chem., Int. Ed.* **2017**, *56*, 8771−8775.
(28) Yang, J.; Song, J. I.; Song, Q.; Rho, J. Y.; Mansfield, E. D. H.; Hall, S. C. L.; Sambrook, M.; Huang, F.; Perrier, S. Hierarchical Self-Assembled Photo-Responsive Tubisomes from a Cyclic Peptide-Bridged Amphiphilic Block Copolymer. *Angew. Chem., Int. Ed.* **2020**, *59*, 8860−8863.
(29) Merg, A. D.; Touponse, G.; Genderen, E. v.; Blum, T. B.; Zuo, X.; Bazrafshan, A.; Siaw, H. M. H.; McCanna, A.; Brian Dyer, R.; Salaita, K.; Abrahams, J. P.; Conticello, V. P. Shape-Shifting Peptide Nanomaterials: Surface Asymmetry Enables pH-Dependent Formation and Interconversion of Collagen Tubes and Sheets. *J. Am. Chem. Soc.* **2020**, *142*, 19956−19968.
(30) Yan, D.; Zhou, Y.; Hou, J. Supramolecular self-assembly of macroscopic tubes. *Science* **2004**, *303*, 65−67.
(31) Cui, H.; Chen, Z.; Zhong, S.; Wooley, K. L.; Pochan, D. J. Block copolymer assembly via kinetic control. *Science* **2007**, *317*, 647−650.
(32) Wang, X.; Guerin, G.; Wang, H.; Wang, Y.; Manners, I.; Winnik, M. A. Cylindrical block copolymer micelles and co-micelles of controlled length and architecture. *Science* **2007**, *317*, 644−647.
(33) Gilroy, J. B.; Gädt, T.; Whittell, G. R.; Chabanne, L.; Mitchels, J. M.; Richardson, R. M.; Winnik, M. A.; Manners, I. Monodisperse cylindrical micelles by crystallization-driven living self-assembly. *Nat. Chem.* **2010**, *2*, 566−570.
(34) Gröschel, A. H.; Walther, A.; Löbling, T. I.; Schacher, F. H.; Schmalz, H.; Müller, A. H. Guided hierarchical co-assembly of soft patchy nanoparticles. *Nature* **2013**, *503*, 247−251.
(35) Qiu, H.; Hudson, Z. M.; Winnik, M. A.; Manners, I. Multidimensional hierarchical self-assembly of amphiphilic cylindrical block comicelles. *Science* **2015**, *347*, 1329−1332.
(36) Mullins, R. D.; Heuser, J. A.; Pollard, T. D. The interaction of Arp2/3 complex with actin: nucleation, high affinity pointed end capping, and formation of branching networks of filaments. *Proc. Natl. Acad. Sci. U.S.A.* **1998**, *95*, 6181−6186.
(37) Pollard, T. D.; Borisy, G. G. Cellular motility driven by assembly and disassembly of actin filaments. *Cell* **2003**, *112*, 453−465.
(38) Campellone, K. G.; Welch, M. D. A nucleator arms race: cellular control of actin assembly. *Nat. Rev. Mol. Cell Biol.* **2010**, *11*, 237−251.
(39) Romero, S.; Le Clainche, C.; Didry, D.; Egile, C.; Pantaloni, D.; Carlier, M.-F. Formin is a processive motor that requires profilin to accelerate actin assembly and associated ATP hydrolysis. *Cell* **2004**, *119*, 419−429.
(40) Linse, S.; Cabaleiro-Lago, C.; Xue, W.-F.; Lynch, I.; Lindman, S.; Thulin, E.; Radford, S. E.; Dawson, K. A. Nucleation of protein fibrillation by nanoparticles. *Proc. Natl. Acad. Sci. U.S.A.* **2007**, *104*, 8691−8696.
(41) Cabaleiro-Lago, C.; Szczepankiewicz, O.; Linse, S. The effect of nanoparticles on amyloid aggregation depends on the protein stability and intrinsic aggregation rate. *Langmuir* **2012**, *28*, 1852−1857.
(42) Álvarez, Y. D.; Fauerbach, J. A.; Pellegrotti, J. V.; Jovin, T. M.; Jares-Erijman, E. A.; Stefani, F. D. Influence of gold nanoparticles on the kinetics of α-synuclein aggregation. *Nano Lett.* **2013**, *13*, 6156−6163.
(43) John, T.; Gladytz, A.; Kubeil, C.; Martin, L. L.; Risselada, H. J.; Abel, B. Impact of nanoparticles on amyloid peptide and protein aggregation: a review with a focus on gold nanoparticles. *Nanoscale* **2018**, *10*, 20894−20913.
(44) Cedervall, T.; Lynch, I.; Lindman, S.; Berggard, T.; Thulin, E.; Nilsson, H.; Dawson, K. A.; Linse, S. Understanding the nanoparticle-protein corona using methods to quantify exchange rates and affinities of proteins for nanoparticles. *Proc. Natl. Acad. Sci. U.S.A.* **2007**, *104*, 2050−2055.
(45) Gladytz, A.; Abel, B.; Risselada, H. J. Gold-Induced Fibril Growth: The Mechanism of Surface-Facilitated Amyloid Aggregation. *Angew. Chem., Int. Ed.* **2016**, *55*, 11242−11246.
(46) Powers, E. T.; Powers, D. L. The kinetics of nucleated polymerizations at high concentrations: amyloid fibril formation near and above the "supercritical concentration". *Biophys. J.* **2006**, *91*, 122−132.
(47) Knowles, T. P. J.; Waudby, C. A.; Devlin, G. L.; Cohen, S. I. A.; Aguzzi, A.; Vendruscolo, M.; Terentjev, E. M.; Welland, M. E.; Dobson, C. M. An analytical solution to the kinetics of breakable filament assembly. *Science* **2009**, *326*, 1533−1537.
(48) Knowles, T. P. J.; Vendruscolo, M.; Dobson, C. M. The amyloid state and its association with protein misfolding diseases. *Nat. Rev. Mol. Cell Biol.* **2014**, *15*, 384−396.
(49) Ferrone, F. [17] Analysis of protein aggregation kinetics. *Methods Enzymol.* **1999**, *309*, 256−274.
(50) Dear, A. J.; Meisl, G.; Michaels, T. C. T.; Zimmermann, M. R.; Linse, S.; Knowles, T. P. J. The catalytic nature of protein aggregation. *J. Chem. Phys.* **2020**, *152*, 045101.
(51) Michaelis, L.; Menten, M. L. Die kinetik der invertinwirkung. *Biochem. Z.* **1913**, *49*, 352.
(52) Deming, T. J. Synthetic polypeptides for biomedical applications. *Prog. Polym. Sci.* **2007**, *32*, 858−875.
(53) Song, Z.; Fu, H.; Wang, R.; Pacheco, L. A.; Wang, X.; Lin, Y.; Cheng, J. Secondary structures in synthetic polypeptides from N-carboxyanhydrides: design, modulation, association, and material applications. *Chem. Soc. Rev.* **2018**, *47*, 7401−7425.
(54) Hadjichristidis, N.; Iatrou, H.; Pitsikalis, M.; Sakellariou, G. Synthesis of Well-Defined Polypeptide-Based Materials via the Ring-Opening Polymerization of α-Amino Acid N-Carboxyanhydrides. *Chem. Rev.* **2009**, *109*, 5528−5578.
(55) Xia, H.; Fu, H.; Zhang, Y.; Shih, K.-C.; Ren, Y.; Anuganti, M.; Nieh, M.-P.; Cheng, J.; Lin, Y. Supramolecular assembly of comb-like macromolecules induced by chemical reactions that modulate the macromolecular interactions in situ. *J. Am. Chem. Soc.* **2017**, *139*, 11106−11116.
(56) Bellomo, E. G.; Wyrsta, M. D.; Pakstis, L.; Pochan, D. J.; Deming, T. J. Stimuli-responsive polypeptide vesicles by conformation-specific assembly. *Nat. Mater.* **2004**, *3*, 244−248.
(57) Chen, C.; Wang, Z.; Li, Z. Thermoresponsive polypeptides from pegylated poly-L-glutamates. *Biomacromolecules* **2011**, *12*, 2859−2863.
(58) Rodríguez-Hernández, J.; Lecommandoux, S. Reversible inside−out micellization of pH-responsive and water-soluble vesicles based on polypeptide diblock copolymers. *J. Am. Chem. Soc.* **2005**, *127*, 2026−2027.
(59) Lu, H.; Cheng, J. Hexamethyldisilazane-Mediated Controlled Polymerization of α-Amino Acid N-Carboxyanhydrides. *J. Am. Chem. Soc.* **2007**, *129*, 14114−14115.
(60) Song, Z.; Fu, H.; Wang, J.; Hui, J.; Xue, T.; Pacheco, L. A.; Yan, H.; Baumgartner, R.; Wang, Z.; Xia, Y.; Wang, X.; Yin, L.; Chen, C.;

https://doi.org/10.1021/acs.biomac.1c01230
Biomacromolecules XXXX, XXX, XXX−XXX

1164 Rodríguez-López, J.; Ferguson, A. L.; Lin, Y.; Cheng, J. Synthesis of
1165 polypeptides via bioinspired polymerization of in situ purified *N*-
1166 carboxyanhydrides. *Proc. Natl. Acad. Sci. U.S.A.* **2019**, *116*, 10658−
1167 10663.
1168 (61) Mahalingam, V.; Onclin, S.; Péter, M.; Ravoo, B. J.; Huskens, J.;
1169 Reinhoudt, D. N. Directed self-assembly of functionalized silica
1170 nanoparticles on molecular printboards through multivalent supra-
1171 molecular interactions. *Langmuir* **2004**, *20*, 11756−11762.
1172 (62) Schiestel, T.; Brunner, H.; Tovar, G. E. M. Controlled surface
1173 functionalization of silica nanospheres by covalent conjugation
1174 reactions and preparation of high density streptavidin nanoparticles.
1175 *J. Nanosci. Nanotechnol.* **2004**, *4*, 504−511.
1176 (63) Bishop, M. F.; Ferrone, F. A. Kinetics of nucleation-controlled
1177 polymerization. A perturbation treatment for use with a secondary
1178 pathway. *Biophys. J.* **1984**, *46*, 631−644.
1179 (64) Cohen, S. I. A.; Linse, S.; Luheshi, L. M.; Hellstrand, E.; White,
1180 D. A.; Rajah, L.; Otzen, D. E.; Vendruscolo, M.; Dobson, C. M.;
1181 Knowles, T. P. J. Proliferation of amyloid-42 aggregates occurs
1182 through a secondary nucleation mechanism. *Proc. Natl. Acad. Sci.*
1183 *U.S.A.* **2013**, *110*, 9758−9763.
1184 (65) Ferrone, F. A. Assembly of Aβ Proceeds via Monomeric Nuclei.
1185 *J. Mol. Biol.* **2015**, *427*, 287−290.
1186 (66) Chen, S.; Ferrone, F. A.; Wetzel, R. Huntington's disease age-
1187 of-onset linked to polyglutamine aggregation nucleation. *Proc. Natl.*
1188 *Acad. Sci. U.S.A.* **2002**, *99*, 11884−11889.
1189 (67) Naiki, H.; Higuchi, K.; Hosokawa, M.; Takeda, T. Fluorometric
1190 determination of amyloid fibrils in vitro using the fluorescent dye,
1191 thioflavine T. *Anal. Biochem.* **1989**, *177*, 244−249.
1192 (68) Krebs, M. R. H.; MacPhee, C. E.; Miller, A. F.; Dunlop, I. E.;
1193 Dobson, C. M.; Donald, A. M. The formation of spherulites by
1194 amyloid fibrils of bovine insulin. *Proc. Natl. Acad. Sci. U.S.A.* **2004**,
1195 *101*, 14420−14424.
1196 (69) Krebs, M. R. H.; Bromley, E. H. C.; Rogers, S. S.; Donald, A.
1197 M. The mechanism of amyloid spherulite formation by bovine insulin.
1198 *Biophys. J.* **2005**, *88*, 2013−2021.
1199 (70) Lehman, S. E.; Tataurova, Y.; Mueller, P. S.; Mariappan, S. V.
1200 S.; Larsen, S. C. Ligand characterization of covalently functionalized
1201 mesoporous silica nanoparticles: An NMR toolbox approach. *J. Phys.*
1202 *Chem. C* **2014**, *118*, 29943−29951.
1203 (71) Stolarczyk, J. K.; Deak, A.; Brougham, D. F. Nanoparticle
1204 clusters: assembly and control over internal order, current capabilities,
1205 and future potential. *Adv. Mater.* **2016**, *28*, 5400−5424.
1206 (72) Levine, H., III Thioflavine T interaction with synthetic
1207 Alzheimer's disease β-amyloid peptides: Detection of amyloid
1208 aggregation in solution. *Protein Sci.* **1993**, *2*, 404−410.
1209 (73) Duan, H.; Luo, Q.; Wei, Z.; Lin, Y.; He, J. Symmetry-Broken
1210 Patches on Gold Nanoparticles through Deficient Ligand Exchange.
1211 *ACS Macro Lett.* **2021**, *10*, 786−790.
1212 (74) Krejtschi, C.; Hauser, K. Stability and folding dynamics of
1213 polyglutamic acid. *Eur. Biophys. J.* **2011**, *40*, 673−685.
1214 (75) Dzwolak, W.; Muraki, T.; Kato, M.; Taniguchi, Y. Chain-length
1215 dependence of α-helix to β-sheet transition in polylysine: Model of
1216 protein aggregation studied by temperature-tuned FTIR spectroscopy.
1217 *Biopolymers* **2004**, *73*, 463−469.
1218 (76) Khurana, R.; Coleman, C.; Ionescu-Zanetti, C.; Carter, S. A.;
1219 Krishna, V.; Grover, R. K.; Roy, R.; Singh, S. Mechanism of thioflavin
1220 T binding to amyloid fibrils. *J. Struct. Biol.* **2005**, *151*, 229−238.
1221 (77) Arad, E.; Green, H.; Jelinek, R.; Rapaport, H. Revisiting
1222 thioflavin T (ThT) fluorescence as a marker of protein fibrillation -
1223 The prominent role of electrostatic interactions. *J. Colloid Interface Sci.*
1224 **2020**, *573*, 87−95.

https://doi.org/10.1021/acs.biomac.1c01230
Biomacromolecules XXXX, XXX, XXX−XXX